

# Vector interaction, charge neutrality and multiple chiral critical point structures

Zhao Zhang\* and Teiji Kunihiro†

*Department of Physics, Kyoto University, Kyoto 606-8502, Japan*

We investigate the combined effect of the repulsive vector interaction and the positive electric chemical potential on the chiral phase transition by considering neutral color superconductivity. The chiral condensate, diquark condensate and quark number densities are solved in both two-flavor and two-plus-one-flavor Nambu-Jona-Lasinio models with the so called Kobayashi-Maskawa-'t Hooft term under the charge-neutrality constraint. We demonstrate that multiple chiral critical-point structures always exist in the Nambu-Jona-Lasinio model within the self-consistent mean-field approximation, and that the number of chiral critical points can vary from zero to four, which is dependent on the magnitudes of vector interaction and the diquark coupling. The difference between the dynamical chemical potentials induced by vector interaction for u and d quarks can effectively reduce the Fermi sphere disparity between the two flavors of diquark pairing. Thus the vector interaction works to significantly suppress the unstable region associated with chromomagnetic instability in the phase of neutral asymmetric homogeneous color superconductivity.

PACS numbers: 12.38.Aw, 11.10.Wx, 11.30.Rd, 12.38.Gc

## I. INTRODUCTION

It is generally believed that QCD exhibits a rich phase structure in an extreme environment such as at high temperature and high baryon chemical potential. For the chiral phase transition, it is a widely accepted view that the critical point(s) (i.e. the end point of the first-order phase boundary) should exist at finite temperature and density. Recently, a schematic  $T$ - $\mu$  phase diagram with one critical point was extensively adopted in the literature[1, 2, 3].

In the last decade the color-superconducting (CSC) phase has attracted a lot of theoretical interest and prompted extensive studies of dense and cold quark matter [4, 5, 6, 7]. At asymptotically high density that justifies the perturbative QCD calculations, the color-flavor locked (CFL) phase [8] has been established as the ground state of quark matter. For the intermediate density region which may exist in the core of a compact star, the nonperturbative features of QCD play a more important role in the phase structure of QCD, and both CFL and non-CFL CSC phases may appear in this region.

The possible emergence of a CFL or a non-CFL CSC phase around the chiral transition boundary at low temperatures should affect the chiral phase transition, and hence the interplay between the chiral condensate and the diquark condensate may result in an unexpected phase structure of QCD. Such an example was first presented in [9] in a two-flavor Nambu-Jona-Lasinio (NJL) model with the vector interaction included: It was found that the repulsive vector interaction can lead to a two-critical-point structure in the  $T$ - $\mu$  phase diagram of QCD, which is due to the fact that the density-density correlation induced by the vector interaction effectively enhances the competition between the chiral and diquark correlations while weakening the first-order chiral restoration[1, 10, 11]. We note that the renormalization-group analysis [12, 13], the chiral instanton-anti-instanton molecule model [14], and the truncated Dyson-Schwinger model of QCD [15] all support the existence of the vector-vector four-quark interaction. The vector-vector interaction may be responsible for the vacuum properties of vector mesons in low-energy effective theories of QCD[16, 17, 18].

In a quite different context, a realization of a similar two-critical-point structure of the QCD phase diagram has been recently conjectured [19]: That is, the  $U_A(1)$ -breaking vertex may induce a new critical point. This conjecture is based on a general Ginzburg-Landau theory constrained by QCD symmetries. There, the three-flavor anomaly term generates the cubic coupling between the chiral and diquark condensates. It has been argued that the resultant crossover of chiral restoration at small temperatures embodies the hadron-quark continuity hypothesis [20]. Further investigation is necessary to clarify whether the new critical point really exists or not with reasonable parameter.

Beside the above two cases, another mechanism which can induce multiple critical-point structure was demonstrated in [21], where it was first disclosed that the positive electric chemical potential  $\mu_e$  required by the charge-neutrality constraint plays a similar role as the repulsive vector interaction on the chiral phase transition in a four-quark

---

\*Electronic address: zhaozhang@pku.org.cn

†Electronic address: kunihiro@ruby.scphys.kyoto-u.ac.jp

interaction model: In a simple two-flavor NJL model, the same two-critical-point structure found in [9] was obtained. In addition, positive  $\mu_e$  also represents the magnitude of disparity between Fermi spheres of u and d quarks when taking into account the local charge-neutrality constraint. For an asymmetric homogeneous system including two different flavor quarks with the mismatched Fermi spheres, the energy gap of the Cooper pairing between these two-flavor quarks can increase with temperature. This unusual behavior of the energy gap is due to the smearing of the Fermi surface by temperature. For the two-flavor neutral CSC phase, this unconventional thermal behavior of the diquark condensate can lead to a special competition between the chiral condensate and the diquark condensate, which may be enhanced with increasing temperature. For some model parameter regions, this abnormal competition induced by  $\mu_e$  can result in a nontrivial three-critical-point phase structure [21]. The competition of two order parameters with the external constraint(s) should also suggest a general mechanism for a realization of a multiple critical-point structure, which may have some implications to study the phase transitions in condensed matter physics.

Note, however, that a very simple two-flavor NJL model with only scalar quark-antiquark and diquark interaction was used in Ref. [21]: If the model produces a relatively large vacuum quark mass, no multiple critical points appear in such formalism even though the charge-neutral constraint is taken into account for the CSC phase. For a more realistic situation, both the vector interaction and the strange quark degree of freedom should be taken into account.

Because in the chiral phase transition similar roles are played by the repulsive vector interaction and the electric chemical potential under the neutrality constraint, one can expect that the chiral restoration will be weakened more significantly when simultaneously taking into account both the ingredients. In this case, it is possible that the multiple critical point structures shown in [21] will become more robust, which we will show in the present work. In addition, for the neutral quark matter system, because of the quark density discrepancy, the vector interaction should also give different contributions to the dynamical chemical potentials for u and d quarks. This may have important influence on the property of the asymmetric homogeneous CSC phase which suffers from the so called chromomagnetic instability characterized by the negative Meissner mass squared [22]. This is a significant observation and will be shown to be the case in the following sections.

There have been extensive studies within the NJL model on the phase diagram of dense and locally neutral three-flavor quark matter with strange quarks explicitly included [23, 24]: In the strong coupling case, the chiral breaking phase at low temperature is bordered by the 2CSC phase, while for the weak coupling case it is surrounded by both normal quark matter and a gapless phase called g2CSC. However, no new critical point was found in [23, 24], in contrast to the result reported in [21]. Notice, however, that the vector interaction was not included in [23, 24], and hence only a strong first-order chiral restoration happened in the low temperature region. We can expect that the qualitative feature of the phase diagram, even for the three-flavor quark matter reported in [23, 24], may change when the repulsive vector interaction is taken into account together with the charge-neutrality constraint. Again, we shall see that this is actually the case, and there appear multiple critical points in the phase diagram of three-flavor quark matter.

The paper is organized as follows. In the next section, a nonlocal two-flavor NJL model is used to investigate the  $(T, \mu)$  phase structure of QCD, with both vector interaction and charge-neutrality being taken into account. The extension of the work to the two-plus-one-flavor case with the so-called Kobayashi-Maskawa-'t Hooft(KMT) term[25] is presented in Sec.III. The final section is devoted to a summary and concluding remarks.

## II. TWO-FLAVOR CASE

We will demonstrate the joint effect of the vector interaction and neutral electric-charge constraint on the QCD phase diagram within a nonlocal two-flavor NJL model.

### A. Model

NJL-type models have been extensively used to investigate the CSC phase transition at moderate and large densities [6]: See the previous study without the CSC [1, 10, 26, 27]. The advantage of a NJL model is that it can investigate the interplay between the chiral condensate, the diquark condensate and the quark number density on the same footing. For the two-flavor case, a nonlocal NJL model [28, 29, 30, 31, 32, 33, 34] is adopted here, which has the Lagrangian density,

$$\begin{aligned} \mathcal{L} = & \bar{\psi}(i\not{\partial} - \hat{m})\psi + G_S \left[ (\bar{q}(x)q(x))^2 + (\bar{q}(x)i\gamma_5\vec{\tau}q(x))^2 \right] - G_V \sum_{i=0}^3 \left[ (\bar{q}(x)\gamma^\mu\tau_i q(x))^2 + (\bar{q}(x)i\gamma^\mu\gamma_5\tau_i q(x))^2 \right] \\ & + G_D \sum_A [\bar{q}(x)\gamma_5\tau_2\lambda_A q_C(x)] [\bar{q}_C(x)\gamma_5\tau_2\lambda_A q(x)], \end{aligned} \quad (1)$$

Parameter set	m(MeV)	$G_S\Lambda^2$	$\Lambda$ (MeV)	$-\langle\bar{u}u\rangle^{1/3}$ (MeV)	$M(p=0)$ (MeV)
Set 1	5.01137	2.64310	600.271	248.440	400
Set 2	4.92671	2.51088	617.968	249.906	367.5
Set 3	4.70805	2.35908	649.168	253.699	330

TABLE I: Model parameter sets for two-flavor nonlocal NJL.

where

$$q(x) = \int dy^4 \tilde{f}(x-y) \psi(y), \quad q_C(x) = \int dy^4 \tilde{f}(x-y) \psi_C(y), \quad \psi_C = C\bar{\psi}^T \quad (2)$$

and  $C = i\gamma_0\gamma_2$  stands for the Dirac charge conjugation matrix. The three coupling constants, namely  $G_S$ ,  $G_V$ , and  $G_D$ , belong to the scalar mesonic channel, the vector mesonic channel, and the diquark channel, respectively. The current quark mass matrix is given by  $\hat{m} = \text{diag}(m_u, m_d)$  in two flavors, and we shall work in the isospin symmetric limit with  $m_u = m_d = m$ . We note that  $\lambda_A$ 's are the antisymmetric Gell-Mann matrices (i.e.  $A$  runs over 2, 5, 7 only) for the color SU(3) group, while  $\tau_0$  and the  $\vec{\tau}$ 's are the unit matrix and Pauli matrices in flavor space, respectively. In contrast to the scalar interaction, the vector part has  $U(2) \times U(2)$  flavor symmetry, and hence the vector terms can be decomposed into  $\sim (\bar{u}\gamma^\mu u)^2 + (\bar{d}\gamma^\mu d)^2$  without the flavor mixing term like  $\bar{u}\gamma^\mu u \bar{d}\gamma_\mu d$ , although there are terms like  $\bar{u}\gamma^\mu d \bar{d}\gamma_\mu u$ .

In contrast to the local NJL model, Lagrangian (1) is formulated with a nonlocal interaction, which is controlled by a form factor  $\tilde{f}(x)$ . This type of model can be considered as a special case of the truncated Dyson-Schwinger equation with a separable effective gluon propagator or an instantaneous nonlocal chiral quark model. The main purpose of adopting such a nonlocal interaction model in our study is to deal with the one-loop ultraviolet divergence, especially for the calculation of the Meissner mass squared at finite temperature [35]. For convenience, we follow the model parametrization in [34] and use the so-called Lorentzian form factor with the form

$$f^2(p = |\mathbf{p}|) = g(p) = \frac{1}{1 + (\frac{p}{\Lambda})^{2a}}, \quad (3)$$

where  $f(p)$  is the Fourier transformation of the form factor  $\tilde{f}(x)$ . In Eq.(3),  $a$  is a dimensionless parameter and  $\Lambda$  stands for the scale parameter of the model. To check the sensitivity of the main results on the model parameter choice, three sets of model parameters are adopted in this paper, which are listed in Tabel.(I)<sup>1</sup> By choosing  $a = 10$ <sup>2</sup>, the other three model parameters, namely  $\Lambda$ ,  $G_S$  and  $m$ , are determined by the vacuum physical quantities of the pion mass  $M_\pi = 135\text{MeV}$ , the pion decay constant  $f_\pi = 92.4\text{MeV}$ , and the quark condensate  $-\langle\bar{u}u\rangle^{1/3} \approx 250\text{MeV}$ . Note that the value of the current quark mass is around 5MeV and the Gell-Mann-Oakes-Renner relation holds well for these parametrizations of the model parameters [34].

In the nonlocal NJL model, the produced constituent quark mass is momentum dependent. Table (I) shows that the vacuum constituent quark mass  $M(p=0)$  ranges from 330 MeV to 400 MeV for the listed three sets of model parameters which almost reproduce the same vacuum physical quantities. Although the vacuum constituent quark mass is not an observable, all the values of  $M(p=0)$  in Table (I) are phenomenologically acceptable because the mass  $3M(p=0)$  is larger than the nucleon mass in the vacuum, which is a bound state of three quarks.

Because there are no reliable constraints on  $G_V$  and  $G_D$  within the two-flavor NJL model, these two model parameters are taken as free parameters in our treatment. The standard ratios of  $G_V/G_S$  and  $G_D/G_S$  from Fierz transformation based on the local color current-current interaction are 0.5 and 0.75, respectively. In addition, in the molecular instanton liquid model, the ratio  $G_V/G_S$  is about 0.25. Combining this point with the Fierz transformation, the reasonable value of  $G_V/G_S$  may be located in the range from 0 to 0.5. In the following numerical calculations, we will focus on the influence of the vector interaction on the phase diagram by varying  $G_V/G_S$  while fixing  $G_D/G_S$  as its standard value. In the literature, such a choice of diquark interaction is usually called the intermediate coupling.

<sup>1</sup> We mention that our results obtained in the Lorentzian nonlocal cutoff scheme are equally obtained even with the traditional sharp cutoff scheme. In this sense, our results, especially the realization of the multiple critical-point structures of the phase diagram are robust and not artificial.

<sup>2</sup> We have checked the main conclusion of this paper is insensitive to a or the form of  $g(p)$  if it can give reasonable vacuum properties of QCD.

## B. Thermodynamic Potential with Neutrality Condition

The grand partition function is given by

$$Z \equiv e^{-\Omega V/T} = \int D\bar{\psi} D\psi e^{i \int d^4x (\mathcal{L} + \psi^\dagger \hat{\mu} \psi)}, \quad (4)$$

where  $\Omega$  is the thermodynamic potential density and  $\hat{\mu}$  is the quark chemical-potential matrix. In general, the quark chemical-potential matrix  $\hat{\mu}$  takes the form [36]

$$\hat{\mu} = \mu - \mu_e Q + \mu_3 T_3 + \mu_8 T_8, \quad (5)$$

where  $\mu$  is the quark chemical potential (i.e. one third of the baryon chemical potential),  $\mu_e$  is the chemical potential associated with the (negative) electric-charge, and  $\mu_3$  and  $\mu_8$  represent the color chemical potentials corresponding to the Cartan subalgebra in color SU(3) space. The explicit form of the electric charge matrix is  $Q = \text{diag}(\frac{2}{3}, -\frac{1}{3})$  in flavor space, and the color charge matrices are  $T_3 = \text{diag}(\frac{1}{2}, -\frac{1}{2}, 0)$  and  $T_8 = \text{diag}(\frac{1}{3}, \frac{1}{3}, -\frac{2}{3})$  in color space. The chemical potentials for different quarks are listed below:

$$\begin{aligned} \mu_{ru} &= \mu - \frac{2}{3}\mu_e + \frac{1}{2}\mu_3 + \frac{1}{3}\mu_8, & \mu_{gu} &= \mu - \frac{2}{3}\mu_e - \frac{1}{2}\mu_3 + \frac{1}{3}\mu_8, \\ \mu_{rd} &= \mu + \frac{1}{3}\mu_e + \frac{1}{2}\mu_3 + \frac{1}{3}\mu_8, & \mu_{gd} &= \mu + \frac{1}{3}\mu_e - \frac{1}{2}\mu_3 + \frac{1}{3}\mu_8, \\ \mu_{bu} &= \mu - \frac{2}{3}\mu_e - \frac{2}{3}\mu_8, & \mu_{bd} &= \mu + \frac{1}{3}\mu_e - \frac{2}{3}\mu_8. \end{aligned} \quad (6)$$

At finite temperature and density, the Lorentz invariance is broken. The three types of four-quark interactions in Eq. (1) could develop three different condensates in a homogeneous phase:  $\sigma_\alpha = \langle \bar{q}_\alpha^a q_\alpha^a \rangle$  (only sum over  $a$ ),  $\Delta = \langle (\bar{q}_C)_\alpha^a i\gamma_5 \epsilon^{\alpha\beta\gamma} \epsilon_{ab3} q_\beta^b \rangle$ , and  $\rho_\alpha = \langle \bar{q}_\alpha^a \gamma^0 q_\alpha^a \rangle$  (only sum over  $a$ ), where the indices  $\alpha$  and  $a$  refer to flavor and color, respectively. The last vector-type condensate appears due to the breaking of Lorentz invariance at finite temperature and density, which corresponds to the quark number density for flavor  $\alpha$ . Here, we follow the common treatment for the two-flavor CSC phase where the blue quarks do not take part in the Cooper pairing.

In the mean-field approximation which we will adopt, it is convenient to introduce the following two gaps and an effective chemical potential corresponding to the above condensates; that is, the dynamical quark mass

$$M(p) = m - 2G_S(\sigma_u + \sigma_d)g(p), \quad (7)$$

the gap for CSC phase

$$\Delta(p) = \Delta g(p), \quad (8)$$

and the dynamical quark chemical potential

$$\tilde{\mu}_\alpha(p) = \mu_\alpha - 4G_V \rho_\alpha g(p). \quad (9)$$

Note that the nonlocal interactions lead to all the gaps being momentum dependent, which is described by  $g(p)$  in the separable model. The advantage of the choice of the separable interaction is that the gap equations can be obtained by the variational method. We also note that the *induced chemical potentials*,  $-4G_V \rho_\alpha g(p)$ , for u and d quarks are different from each other due to the constraint of electric charge neutrality ( $\mu_d > \mu_u$  and hence  $\rho_d > \rho_u$ ); notice also, however, that they are dependent only on the respective density  $\rho_{u,d}$ , and hence the dynamical chemical potentials  $\tilde{\mu}_{u,d}(p)$  tend to come closer because  $\rho_d > \rho_u$  with the common coupling constant  $G_V$ .

Using the standard bosonization technique, the mean-field thermodynamic potential in the NJL model with the electron contribution takes the following form:

$$\Omega = \Omega_L - T \sum_n \int \frac{d^3p}{(2\pi)^3} \text{Tr} \ln \frac{S_{\text{MF}}^{-1}(i\omega_n, \vec{p})}{T} + \Omega_C, \quad (10)$$

where

$$\Omega_L = 2G_S(\sigma_u^2 + \sigma_d^2) - 2G_V(\rho_u^2 + \rho_d^2) + \frac{\Delta^2}{4G_D} - \frac{1}{12\pi^2} \left( \mu_e^4 + 2\pi^2 T^2 \mu_e^2 + \frac{7\pi^4}{15} T^4 \right), \quad (11)$$

and the sum runs over the Matsubara frequency  $\omega_n = (2n+1)\pi T$  and Tr is taken over color, flavor, and Dirac indices. The last term in (11) is the contribution of the free electron gas. Note that a UV divergent counter part  $\Omega_C$  is introduced in (10) due to the one-loop integration.

The inverse quark propagator matrix in the Nambu-Gor'kov formalism is given by

$$S_{\text{MF}}^{-1}(i\omega_n, \vec{p}) = \begin{pmatrix} [G_0^+]^{-1} & \Delta\gamma_5\tau_2\lambda_2 \\ -\Delta^*\gamma_5\tau_2\lambda_2 & [G_0^-]^{-1} \end{pmatrix}, \quad (12)$$

with

$$[G_0^\pm]^{-1} = \gamma_0(i\omega_n \pm \hat{\mu}(p)) - \vec{\gamma} \cdot \vec{p} - \widehat{M}(p). \quad (13)$$

Taking the Matsubara sum, we can express the thermodynamic potential as usual as

$$\Omega(\mu_e, \mu_3, \mu_8, \sigma, \nu, \Delta; \mu, T) = \Omega_L - \sum_{i=1}^{12} \int \frac{d^3p}{(2\pi)^3} \{ (E_i - E_i^0) + 2T \ln(1 + e^{-E_i/T}) \}, \quad (14)$$

with the dispersion relations for six quasi-particles (that is, 2 flavors  $\times$  3 colors; the spin degeneracy is already taken into account in Eq. (14)) and six quasi-anti-particles. In Eq.(14), the counter part corresponds to

$$\Omega_C = \sum_{i=1}^{12} \int \frac{d^3p}{(2\pi)^3} E_i^0, \quad (15)$$

where  $E_i^0 = E_i(M = m, \Delta = 0, \rho = 0)$ . The unpaired blue quarks have the following four energy dispersion relations,

$$E_{bu} = E - \tilde{\mu}_{bu}, \quad \bar{E}_{bu} = E + \tilde{\mu}_{bu}, \quad E_{bd} = E - \tilde{\mu}_{bd}, \quad \bar{E}_{bd} = E + \tilde{\mu}_{bd} \quad (16)$$

with  $E = \sqrt{\vec{p}^2 + M^2(p)}$ . In the *rd-gu* quark sector with pairing we can find the four dispersion relations,

$$\begin{aligned} E_{rd-gu}^\pm &= E_\Delta \pm \frac{1}{2}(\tilde{\mu}_{rd} - \tilde{\mu}_{gu}) = E_\Delta \pm \delta\tilde{\mu}, \\ \bar{E}_{rd-gu}^\pm &= \bar{E}_\Delta \pm \frac{1}{2}(\tilde{\mu}_{rd} - \tilde{\mu}_{gu}) = \bar{E}_\Delta \pm \delta\tilde{\mu}, \end{aligned} \quad (17)$$

and the *ru-gd* sector has another four as follows:

$$\begin{aligned} E_{ru-gd}^\pm &= E_\Delta \pm \frac{1}{2}(\tilde{\mu}_{ru} - \tilde{\mu}_{gd}) = E_\Delta \mp \delta\tilde{\mu}, \\ \bar{E}_{ru-gd}^\pm &= \bar{E}_\Delta \pm \frac{1}{2}(\tilde{\mu}_{ru} - \tilde{\mu}_{gd}) = \bar{E}_\Delta \mp \delta\tilde{\mu}, \end{aligned} \quad (18)$$

where  $E_\Delta = \sqrt{(E - \tilde{\mu})^2 + \Delta(p)^2}$  and  $\bar{E}_\Delta = \sqrt{(E + \tilde{\mu})^2 + \Delta(p)^2}$ . The average chemical potential is defined by

$$\bar{\mu} = \frac{\tilde{\mu}_{rd} + \tilde{\mu}_{gu}}{2} = \frac{\tilde{\mu}_{ru} + \tilde{\mu}_{gd}}{2} = \mu - \frac{\mu_e}{6} - 2G_V(\rho_u + \rho_d)g(p) + \frac{\mu_8}{3}, \quad (19)$$

and the effective mismatch between the chemical potentials of the u quark and the d quark takes the form

$$\delta\tilde{\mu} = \frac{1}{2}(\mu_e - 4G_V(\rho_d - \rho_u)g(p)). \quad (20)$$

We notice that the vector interaction coupled to the difference of the u and d quark densities tends to diminish the mismatch in the chemical potentials. This effect will play an important role for avoiding the color magnetic instability: see below for further discussions.

For the two-flavor CSC phase,  $\mu_3$  always remains zero due to the left unbroken color SU(2) symmetry for red and green quarks. Minimizing the thermodynamic potential (14), we can solve the mean fields  $\sigma$ ,  $\Delta$ ,  $\rho_{u[d]}$  together with the chemical potential  $\mu_e$  and  $\mu_8$  from

$$\frac{\partial\Omega}{\partial\sigma} = \frac{\partial\Omega}{\partial\Delta_3} = \frac{\partial\Omega}{\partial\rho_u} = \frac{\partial\Omega}{\partial\rho_d} = \frac{\partial\Omega}{\partial\mu_e} = \frac{\partial\Omega}{\partial\mu_8} = 0, \quad (21)$$

where  $\sigma = \sigma_u = \sigma_d$  as demonstrated in [21]. Since  $\mu_8$  is very small for color neutralized two-flavor CSC matter, ignoring this term has a little effect on the phase structure<sup>3</sup>. Considering this point, Eq.(29) is then simplified as a series of five coupling equations.

---

<sup>3</sup> We have checked that the explicit introduction of  $\mu_8$  does not alter the result that the multiple critical-point structures are realized, although there is a slight change in the parameter window for realizing them. It is rather amazing because the value of  $\mu_8$  can be in the same order as that of the induced chemical potential near the phase boundary. The reason of the robustness of the multiple critical-point structures lies in the fact that such phase structures are mainly driven by the competition between the chiral condensate and the diquark condensate in the coexisting region while nonzero  $\mu_8$  has little effect on this competition. The contributions of  $\mu_8$  to the red and green quark chemicals have a negative value,  $\mu_8/3$ , while that to the blue quark has a positive value,  $-\mu_8/3$  with a doubled absolute value, implying that the effect of  $\mu_8$  on the quark mass and diquark condensate tends to cancel with each other.

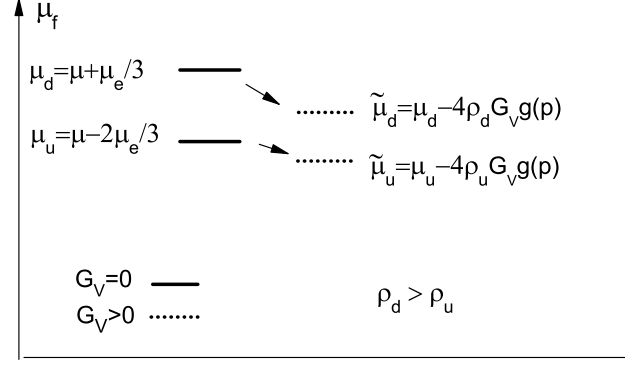


FIG. 1: Effect of the vector interaction on the chemical-potential disparity between the u quark and the d quark. Notice that the amount of the decrease from the chemical potential to the effective chemical potential  $\tilde{\mu}_{u,d}$  is proportional to the respective density  $\rho_{u,d}$  and hence the difference between the effective chemical potentials becomes significantly smaller.

To determine the region of the unstable homogeneous CSC phase associated with magnetic instability, one need to calculate the Meissner masses squared which may be negative with charge neutrality. Here we adopt the same method as in [35] to evaluate the Meissner mass squared

$$m_M^2 = \frac{\partial^2}{\partial B^2} [\Omega(\Delta) - \Omega(\Delta = 0)]_{B=0}, \quad (22)$$

where  $B$  has the same meaning as in [35]. In our calculation, the upper limit of the momentum integration in Eq.(22) is infinity, which helps to avoid the cut-off sensitivity for the evaluation of the Meissner masses encountered in the conventional local NJL model [35].

Note that there are three main changes induced by the nonzero vector-type quark condensates in comparison to the case without vector interactions [21]. First, it give new negative contributions to the thermal potential, which favors the phase with relatively larger dynamical quark mass. This effect becomes more significant when the quark number density is sizable. Second, it give rise to a negative dynamical chemical potential, which can delay the chiral restoration towards larger chemical potential to drive the formation of the coexistence (COE) phase with both the  $\chi$ SB and the CSC phase. In the COE region, the competition between the corresponding order parameters can significantly weaken the first-order chiral phase transition. Third, as shown in Fig.1 and briefly mentioned above, the disparity between the densities of u and d quarks can effectively suppress the chemical-potential mismatch between these two flavors, which might partially or even totally cure the chromomagnetic instability. More details of the influences of the vector interaction combined with the electric-charge neutrality on the phase of QCD will be given in the next subsection.

### C. NUMERICAL RESULTS AND DISCUSSIONS

In this subsection, we shall discuss the effect of vector interaction combined with the charge-neutrality and  $\beta$  equilibrium on both the chiral phase transition and the instability of the CSC phase. Two points will be stressed below: In general, the model parameter window always exists in the NJL model, which favors the multiple critical-point structures, and the number of the critical points can be zero, one, two, three, and even four; the different dynamic chemical potentials induced by the vector interaction for u and d quarks can effectively shrink the unstable homogeneous CSC region towards lower temperatures and larger chemical potentials.

#### 1. Multiple critical-point structures for chiral restoration

In the subsequent subsections we shall present numerical results and see that what is described above is actually the case. For convenience, we shall adopt the same notations as those in Refs. [19, 21] to distinguish the different regions in the  $T$ - $\mu$  phase diagram: NG, CSC, COE, and NOR refer to the hadronic (Nambu-Goldstone) phase with

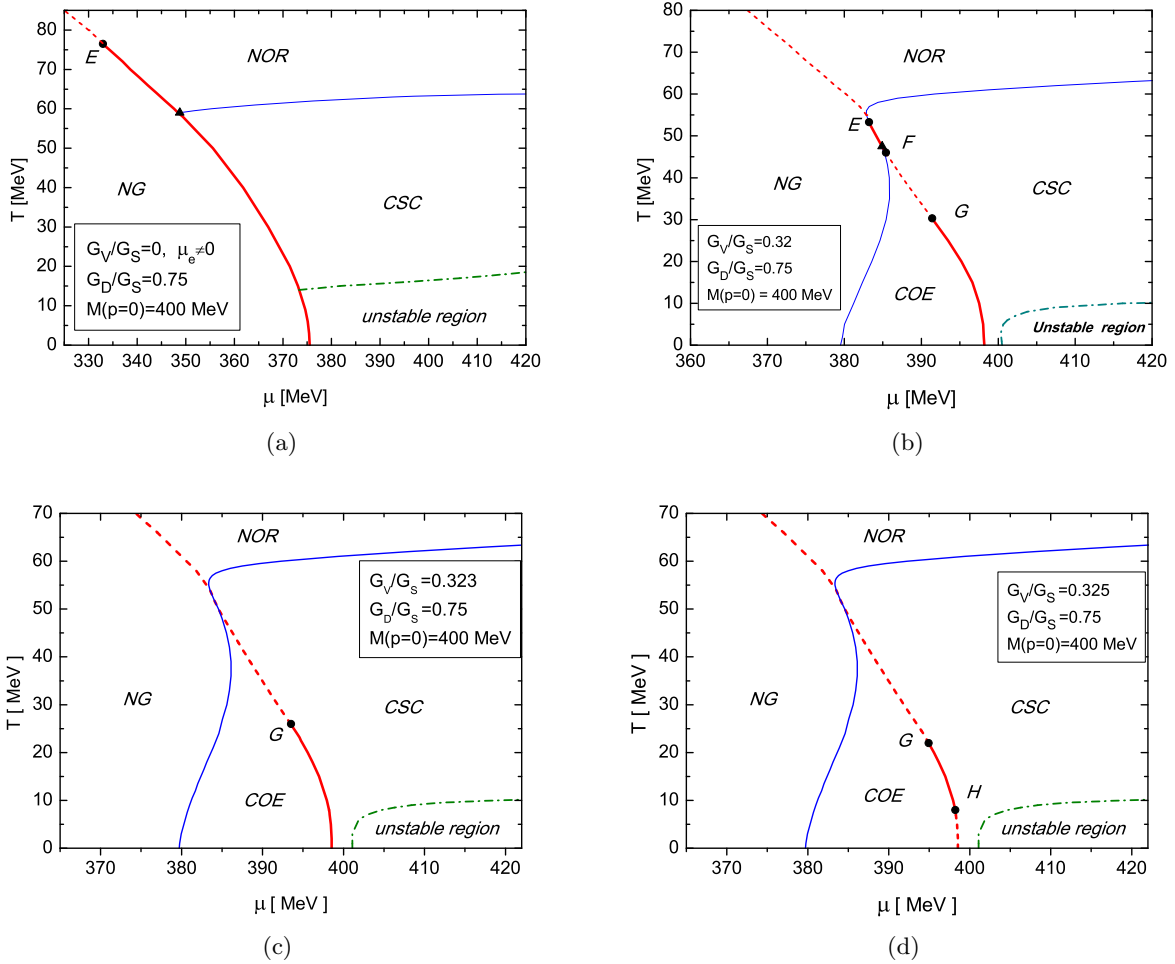


FIG. 2: The phase diagrams for model parameter set 1 with varying  $G_V/G_S$  and fixed  $G_D/G_S = 0.75$ . NG, CSC, COE, and NOR refer to the hadronic (Nambu-Goldstone), color-superconducting, coexisting and normal phase, respectively. The boundary of the unstable region from the chromomagnetic instability is indicated by the dash-dotted curve. With the increase of  $G_V/G_S$ , the number of critical points changes and the instability region tends to shrink toward the lower  $T$  and higher  $\mu$  region in the phase diagram.

$\sigma \neq 0$  and  $\Delta = 0$ , the color-superconducting phase with  $\Delta \neq 0$  and  $\sigma = 0$ , the coexisting phase with  $\sigma \neq 0$  and  $\Delta \neq 0$ , and the normal phase with  $\sigma = \Delta = 0$ , respectively, though they have exact meanings only in the chiral limit.

In Ref. [21], four types of critical-point structures were found with varying diquark coupling constant. We will change the value of the vector coupling  $G_V/G_S$  while fixing the diquark coupling at a standard value. The vector coupling constant in the vacuum may be determined by the vacuum properties of vector mesons. Since the usually adopted scale parameter in the two-flavor NJL model is less than the minimum vacuum mass of vector mesons, one could not get a reliable vector coupling constant within such formalism; on the other hand, the vector coupling constant should also be a function of temperature and quark chemical potential, which is also unknown at the moment. Therefore, to observe the possible effect of vector interaction on the phase transition, the vector coupling constant  $G_V/G_S$  is treated as a free parameter rather than a fixed parameter in the model at hand.

The phase diagrams for parameter set 1 in Table I with different values of  $G_V/G_S$  are shown in Fig. 2. Parameter set 1 corresponds to a relatively large vacuum constituent quark mass,  $M(p=0) = 400 \text{ MeV}$ . Figure 2a indicates that chiral restoration at low temperature keeps a first-order transition, and only a single chiral critical point appears in the phase diagram with vanishing vector interaction. In contrast to the case with the same  $G_D/G_S$  in [21], the first-order chiral transition is too strong to favor the appearance of the COE even though the finite  $\mu_e$  significantly moves the boundary of chiral restoration towards larger  $\mu$  as shown in Fig. 3. With nonzero  $G_V/G_S = 0.32$ , however, Fig. 2b shows that COE emerges and a three-critical-point structure for the chiral transition is realized. This result further verifies the conclusion in Ref. [21] that the abnormal thermal behavior of the energy gap for the mismatched

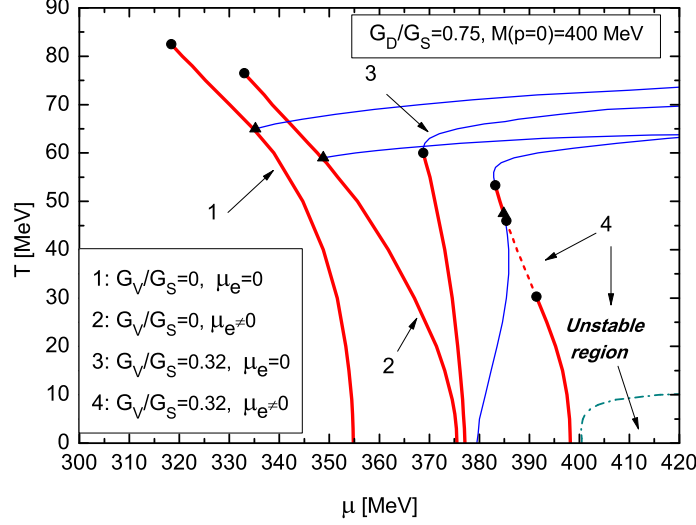


FIG. 3: Chiral phase transitions for model parameter set 1: Numbers 1, 2, 3, and 4 correspond to the cases with vanishing  $G_V$  and no charge-neutrality constraint, vanishing  $G_V$  and a charge-neutrality constraint,  $G_V/G_S = 0.32$  and no charge-neutrality constraint, and  $G_V/G_S = 0.32$  and a charge-neutrality constraint, respectively. The standard value  $G_D/G_S = 0.75$  is adopted in all cases.

diquark pairing can give rise to two new critical points in the low temperature region. We notice that Fig. 2b has a similar phase structure to that given in Fig. 4b of [21], and the mechanism to realize this structure is understood much the same way: The first-order transition line E-F is the remnant of the chiral transition without the CSC phase, which tends to cease to exist at high temperature, while the other first-order transition line ending at G is the chiral transition that survives the effect of a rather strong diquark condensate at low temperatures. In addition, Fig. 2b also shows that all three critical points are free from the chromomagnetic instability.

Note that the vector interaction with  $G_V/G_D = 0.32$  is not yet strong enough to lead to the emergence of COE without the help of the constraint of electric-charge-neutrality, as indicated in Fig. 3. In contrast to the case without both  $G_V$  and the constraint of electric charge, Fig. 3 shows that the critical chemical potential for the chiral transition at zero temperature is delayed towards larger  $\mu$  by about 42 MeV by nonzero  $G_V$  and  $\mu_e$ . Therefore, the combined influence of these two elements on the chiral transition is quite significant.

By further increasing  $G_V$ , Fig. 2d shows that the remnant first-order chiral transition turns into a crossover and the surviving first-order transition still exists with the emergence of another new end point, H. This is quite different from the result in Ref. [21] that the surviving part of the first boundary initially vanishes with increasing  $G_D$ . The reason for the difference is that the relatively large vector interaction has more significant impact on the location of the critical point E, which shifts to lower  $T$  and larger  $\mu$  and eventually is eaten by the enlarged COE. This point is also indicated clearly in Fig. 3. The appearance of H is due to the stronger competition between the chiral condensate and the diquark condensate at lower temperatures. Note that the two critical points in Fig. 2d are also free from the chromomagnetic instability. Figure 2c indicates that one critical-point structure appears again in a very narrow parameter region of the vector coupling, where the first-order line only contains the surviving part.

For larger vector coupling, the chiral boundary will totally become crossover, which is not shown in Fig. 2. In conclusion, with parameter set 1 and  $G_D/G_S = 0.75$ , five types of critical-point structures with critical-point numbers 1, 3, 1, 2, and 0 are found in the model when  $G_V/G_S$  is varied in the range 0 – 0.5. In contrast to the situation in Ref. [21], all the multiple critical points obtained with parameter set 1 are far from the unstable homogeneous CSC region.

The phase diagrams for parameter set 2 with varying  $G_V/G_S$  are shown in Fig. 4. Compared to parameter set 1, the resulting vacuum quark mass  $M(p = 0)$  is reduced and the first-order chiral transition is not very strong. For vanishing  $G_V$ , Fig. 4a gives a similar phase diagram as Fig. 2a. When  $G_V/G_S$  is increased to 0.253, Fig. 2b tells us that a new critical point, H, appears at a very low temperature. This is not surprising since the larger the diquark condensate in the COE phase, the more suppressed the chiral condensate in the lower  $T$  and larger  $\mu$  region, where the phase change is a crossover. With the further increased vector coupling, Fig. 4c shows that *four* critical points appear on the chiral boundary: Owing to the abnormal  $T$  dependence of the diquark condensate, two new critical

points denoted by F and G exist in the phase diagram. Because the vector interaction is not as strong as the case in Fig.2c, both the remnant and the surviving first-order chiral transition remain in the phase diagram. One can see from Fig.4b and Fig.4c that the critical point labeled as H is located on the border between the stable region and the unstable region, while other critical points are free from the chromomagnetic instability. In Fig.4d, with much larger  $G_V/G_S$ , the surviving first-order transition in the lower  $T$  region can not survive anymore, and only the remnant first-order transition in the high  $T$  region is left on the chiral boundary. Therefore, for parameter set 2 and the standard diquark coupling, five types of chiral critical point structures also exist, and the order of the number of the critical points is 1,2,4,2,0 with increasing vector interaction.

In Table II, model parameter set 3 reproduces the smallest vacuum dynamical quark mass, and the corresponding first-order chiral transition is also the weakest one. Figure.5a shows that only finite  $\mu_e$  is capable of realizing the COE in the phase diagram, even though the competition between the chiral and CSC correlations in the COE is not strong enough to lead to a multiple critical-point structure. With the help of vector interaction, the three- and two-critical-point structures appear in Figs. 5b and 5c, respectively. In contrast to the former two cases, only a very small vector interaction can lead to multiple critical-point structures.

Since all the critical-point structures mentioned above are obtained within the range  $G_V/G_S < 0.35$ , one can expect that similar results may be obtained for a relatively weak diquark coupling with the vector coupling varying in the range  $0 < G_V/G_S < 0.5$ . In general, at least in the two-flavor NJL model, we can conclude that there always exists a region in the parameters plane of  $G_D$ - $G_V$  which favors a multiple chiral-critical-point structure, with color superconductivity and electric neutrality being taken into account.

Here it is worth emphasizing that the abnormal  $T$  dependence of the diquark condensate is a general feature in the COE region, even though the same behavior only happens in the CSC dominant region with a weak diquark coupling. The reason is that the quark Fermi surface in the COE is relatively small due to the sizable quark mass. Note that, the various critical-point structures demonstrated above are realized in a very simple chiral quark model of QCD with the physical constraint of charge neutrality. Because of the complexity of QCD, it is possible that there are more than one chiral critical point in the true QCD phase diagram.

## 2. Suppressing the chromomagnetic instability

It is well known that the asymmetric homogeneous g2CSC phase suffers from the chromomagnetic instability. At zero temperature, the calculation based on the hard-dense-loop method [22] suggests that the Meissner mass squared of the 8th gluon becomes negative for  $\frac{\delta\mu}{\Delta} > 1$  while the 4th-7th gluons acquire negative Meissner masses squared for  $\frac{\delta\mu}{\Delta} > 1/\sqrt{2}$ . Note that without the vector interaction, the chemical-potential mismatch  $\delta\mu$  is just equal to  $\mu_e/2$ . The instability of the homogeneous CSC phase should imply the existence of a yet unknown but stable phases in this region of the phase diagram. Such examples proposed so far include the Larkin-Ovchinnikov-Fulde-Ferrel (LOFF) phase [37] and the gluonic phase [38].

Because the Fermi surface is smeared by finite temperature, the homogeneous neutral two-flavor CSC phase can be stable in a somewhat higher temperature region [35, 39, 40]. The same thing happens for the homogeneous neutral CFL phase with three flavors [41]. It is also reported in Ref.[42] that a large quark mass and a strong coupling can effectively suppress the instability even at zero temperature. Here we will demonstrate that the repulsive vector interaction can also resolve or suppress the instability problem. The reason is very simple: According to Eq. (20), the density mismatch between u and d quarks gives a negative contribution to  $\delta\mu$ , which can effectively suppress the ratio  $\delta\mu/\Delta$ .

The ratio  $\delta\mu/\Delta$  (here the ratio  $\delta\mu/\Delta$  refers to  $\delta\mu(p=0)/\Delta(p=0)$ ) as a function of  $\mu$  with fixed  $T = 5\text{MeV}$  for different  $G_V/G_S$  is shown in Fig.6a, where model parameter set 2 is used with  $G_D/G_S = 0.75$ . One can see that  $\delta\mu/\Delta$  significantly decreases with an increasing vector coupling. The regions of the chromomagnetic instability for the corresponding  $G_V/G_S$  are shown in Fig.6b. With increasing  $G_V/G_S$ , the unstable region shrinks towards a lower-temperature and higher chemical-potential region. Actually, we have already seen that the same phenomenon occurs in the phase diagrams of Figs.2-5.

We should notice here that, as seen from Eq.(27), the repulsive vector interaction also suppresses the magnitude of the diquark condensate due to the reduced effective quark chemical potential. However, the direct effect of the vector interaction on  $\delta\mu$  is more significant than that on  $\Delta$ , in particular for finite temperature. We stress that this important role of the vector interaction in the CSC phase, especially for the instability problem, was first revealed in this work. Of course, the vector interaction may not totally remove the unstable region from the phase diagram unless the diquark and/or vector coupling are very large. Therefore, other mechanism may still be necessary for a thorough cure of the magnetic instability.

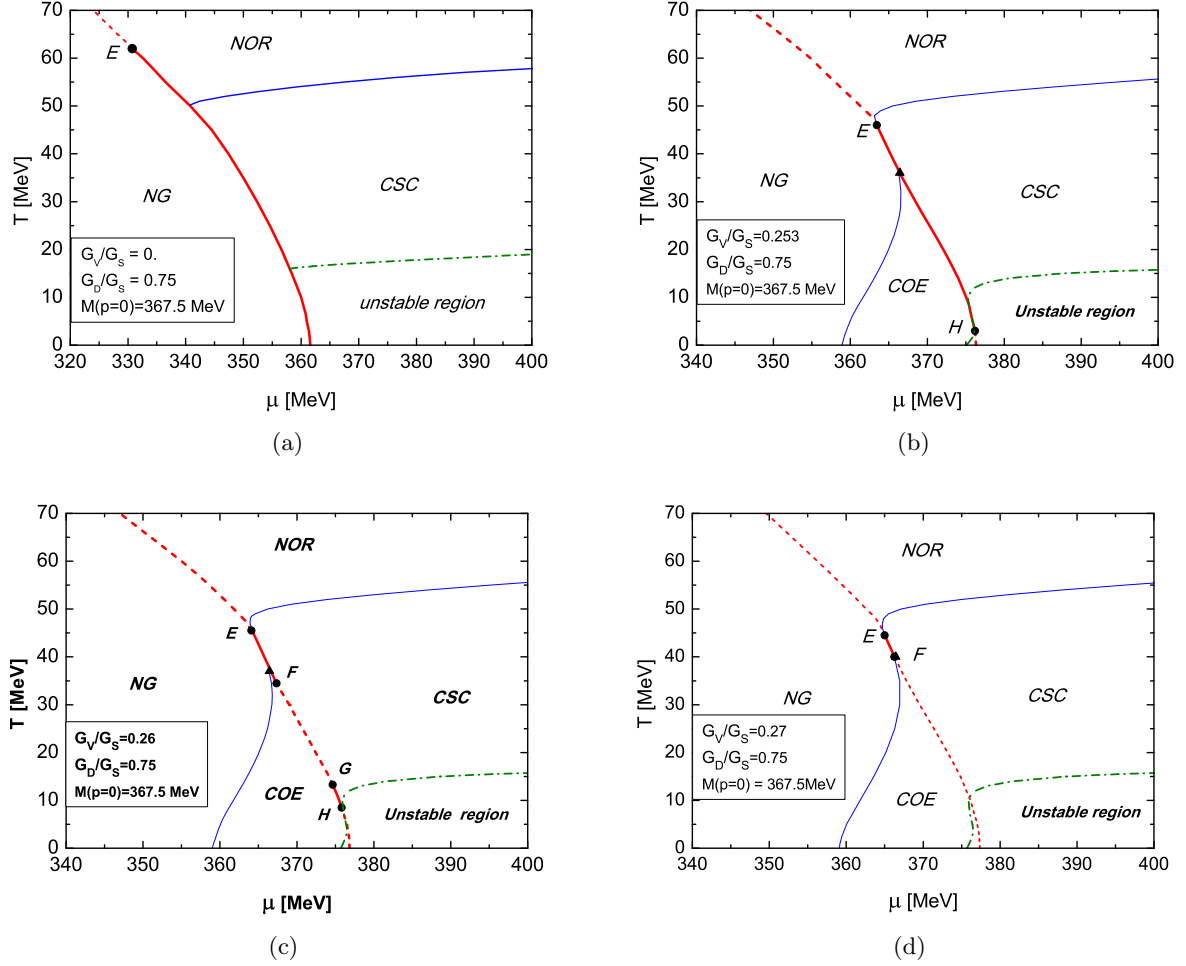


FIG. 4: The phase diagrams for model parameter set 2 with varying  $G_V/G_S$  and fixed  $G_D/G_S = 0.75$ . The unstable region with chromomagnetic instability is indicated by the dash-dotted curve.

### III. TWO-PLUS-ONE-FLAVOR CASE

In this section, the study of the influence of the vector interaction on the chiral phase transition is extended to the two-plus-one-flavor NJL formalism.

#### A. Model

In this part, for simplicity, a local two-plus-one-flavor NJL model is adopted. The two-plus-one-flavor NJL model was developed in the mid-1980s [17, 43, 44], and the most popular version includes a chiral symmetric four-quark interaction term and a determination term [25] in flavor space [45, 46, 47]. To compare with the previous study, we take the same model parameters as in Ref.[23] by including the vector interaction channel. The corresponding Lagrangian density is given by

$$\begin{aligned}
 \mathcal{L} = & \bar{\psi} (i\not{\partial} - \hat{m})\psi + G_S \sum_{i=0}^8 \left[ (\bar{\psi}\lambda_i\psi)^2 + (\bar{\psi}i\gamma_5\lambda_i\psi)^2 \right] - G_V \sum_{i=0}^8 \left[ (\bar{\psi}\gamma^\mu\lambda_i\psi)^2 + (\bar{\psi}i\gamma^\mu\gamma_5\lambda_i\psi)^2 \right] \\
 & + G_D \sum_{\gamma,c} \left[ \bar{\psi}_\alpha^a i\gamma_5 \epsilon^{\alpha\beta\gamma} \epsilon_{abc} (\psi_C)_\beta^b \right] \left[ (\bar{\psi}_C)_\rho^r i\gamma_5 \epsilon^{\rho\sigma\gamma} \epsilon_{rsc} \psi_\sigma^s \right] - K \left\{ \det_f [\bar{\psi} (1 + \gamma_5) \psi] + \det_f [\bar{\psi} (1 - \gamma_5) \psi] \right\}, \quad (23)
 \end{aligned}$$

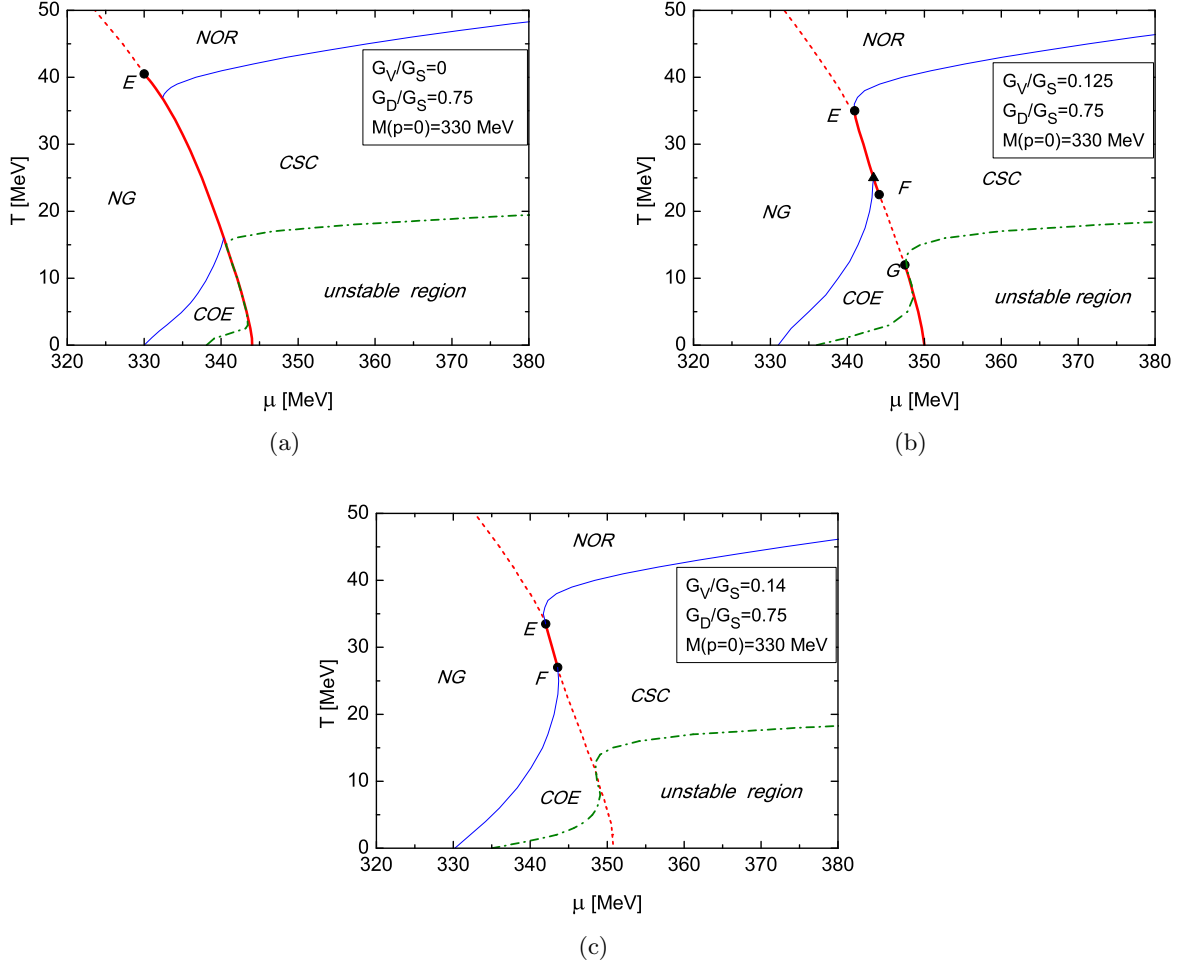


FIG. 5: The phase diagrams for model parameter set 3 with varying  $G_V/G_S$  and fixed  $G_D/G_S = 0.75$ . The unstable region with chromomagnetic instability is indicated by the dash-dotted curve.

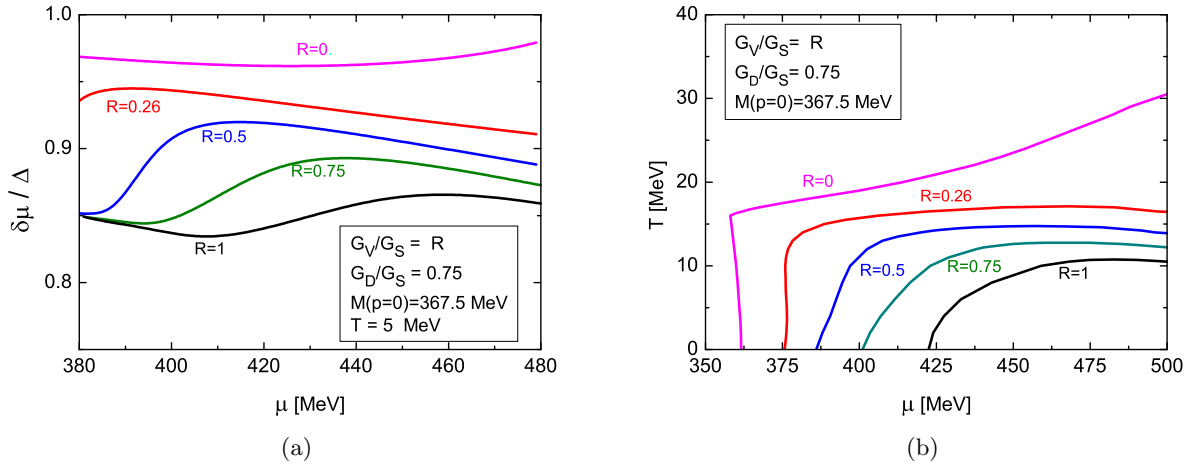


FIG. 6: The effect of the repulsive vector interaction on the ratio  $\delta\mu/\Delta$  (left figure) and the location of the boundary between the stable and unstable homogeneous regions (right figure). With the increase of the ratio  $G_V/G_S \equiv R$ ,  $\delta\mu/\Delta$  tends to become smaller and the unstable region in the  $T$ - $\mu$  plane shrinks toward a lower  $T$  and higher  $\mu$  region.

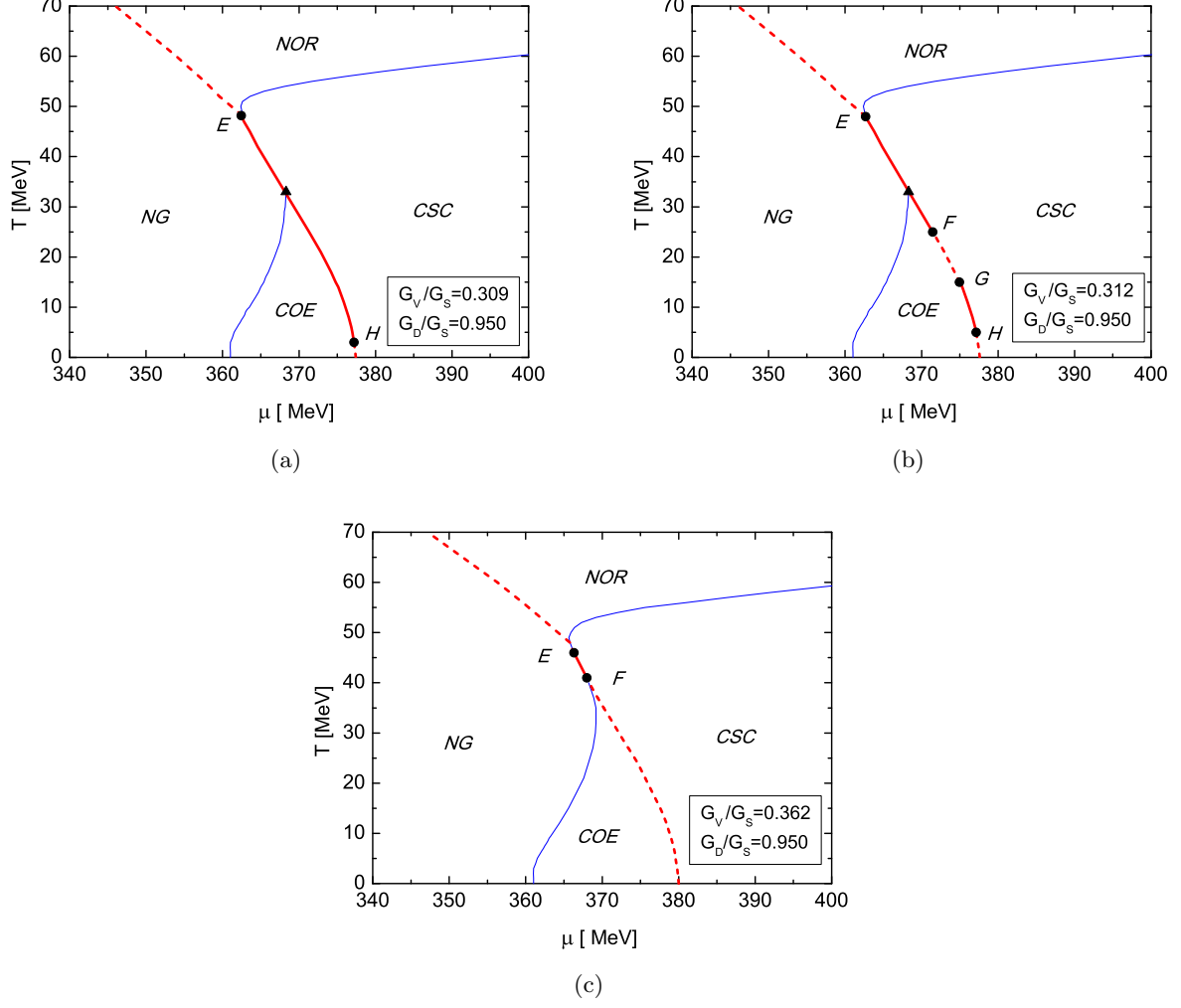


FIG. 7: The phase diagrams for the two-plus-one-flavor NJL model with varying  $G_V/G_S$  and fixed  $G_D/G_S = 0.95$ . Electric-charge-neutrality is considered, and only phase diagrams with multiple chiral critical points are shown.

$m_{u,d}(\text{MeV})$	$m_s(\text{MeV})$	$G_S \Lambda^2$	$K \Lambda^5$	$\Lambda$ (MeV)	$M_{u,d}$ (MeV)
5.5	140.7	1.835	12.36	602.3	367.7
$f_\pi(\text{MeV})$	$m_\pi(\text{MeV})$	$m_K$ (MeV)	$m_{\eta'}$ (MeV)	$m_\eta(\text{MeV})$	$M_s$ (MeV)
92.4	135	497.7	957.8	514.8	549.5

TABLE II: Model parametrization of the two-plus-one-flavor NJL model.

where the quark spinor field  $\psi_\alpha^a$  carries color ( $a = r, g, b$ ) and flavor ( $\alpha = u, d, s$ ) indices. In contrast to the two-flavor case, the matrix of the quark current masses is given by  $\hat{m} = \text{diag}_f(m_u, m_d, m_s)$  and the Pauli matrices in flavor space are replaced by the Gell-Mann matrices  $\lambda_i$  in flavor space with  $i = 1, \dots, 8$ , and  $\lambda_0 \equiv \sqrt{2/3} \mathbb{1}_f$ . The corresponding parametrization of the model parameters is given in Table(II), where  $G_S$ , the coupling constant for the scalar meson channel, and  $K$ , the coupling constant responsible for the  $U_A(1)$  breaking, or the KMT term[25], are fixed by the vacuum physical observables. The other two coupling constants,  $G_V$  and  $G_D$ , are still taken as free parameters in the following.

### B. Thermodynamic potential for neutral color superconductivity

In general, there exist nine possible two-quark condensates for the two-plus-one-flavor case with the Lagrangian (23): three chiral condensates  $\sigma_\alpha$ , three diquark condensates  $\Delta_c$ , and three vector quark condensates  $\rho_\alpha$ , where  $\alpha$  and  $c$  range from 1 to 3, which stand for three flavors and three colors, respectively. At the mean-field level, the thermodynamic potential for the two-plus-one-flavor NJL model including the charge-neutrality constraints, is

$$\begin{aligned} \Omega = & \Omega_l + \frac{1}{4G_D} \sum_{c=1}^3 |\Delta_c|^2 - 2G_V \sum_{\alpha=1}^3 \rho_\alpha^2 + 2G_S \sum_{\alpha=1}^3 \sigma_\alpha^2 \\ & - 4K\sigma_u\sigma_d\sigma_s - \frac{T}{2V} \sum_K \ln \det \frac{S_{MF}^{-1}}{T}, \end{aligned} \quad (24)$$

where  $\Omega_l$  stands for the contribution from free leptons. Note that, for consistency,  $\Omega_l$  should include the contributions from both electrons and muons. Since  $M_\mu \gg M_e$  and  $M_e \approx 0$ , ignoring the contribution from muons has little effect on the phase structure. Therefore, we use  $\Omega_l$  given by the last term in Eq. (11).

It should be stressed here that, for simplicity, the contributions of the cubic mixing terms among three different condensates, such as  $\sigma\Delta^2$ ,  $\rho\Delta^2$ , and  $\sigma\rho^2$ , are neglected in Eq. (24). These terms arise from the KMT interaction which may or may not affect the phase structure. In particular it was argued in [19] that the cubic mixing term between chiral and diquark condensates may play an important role in the chiral phase transition in the low temperature region. Beside the direct contribution of these cubic terms to the thermodynamic potential, the flavor mixing terms arising from the KMT interaction also have influence on the dispersion relationship of quasiquarks. For example, both the diquark condensate and the quark number density contribute to the dynamical quark mass. Therefore, it is a very interesting topic to investigate the possible effect of these cubic coupling terms on the phase diagram by using dynamic models of QCD. Leaving the discussion of this interesting problem to our future work, here we just simply assume that none of these mixing terms makes a qualitative difference in the phase diagram.

Because of the large mass disparity between the strange quark and the u (d) quark, the favored phase at low temperature and moderate density might be 2CSC phase rather than CFL as demonstrated in the two-plus-one-flavor NJL model[23, 24]. These studies suggest that the strange quark mass is close to or even larger than  $\mu$  near the chiral boundary, which means that the strange quark density is considerably smaller than that of the u and d quarks. Therefore, for the two-plus-one-flavor case, the light quarks still play the dominant role around the chiral boundary, and the density mismatch between u and d quarks under the electric-charge-neutrality constraint is still similar to the two-flavor case. Since the main purpose of our study is to investigate the influence of the neutral CSC phase on the chiral phase transition by taking into account the vector interaction, we only consider the 2CSC phase in the following.

The inverse quark propagator in the 2CSC phase in the two-plus-one-flavor case still takes the same form as  $S_{MF}^{-1}$ , with the extended matrixes  $\hat{\mu}$  and  $\hat{M}$  in three-flavor space. The constituent quark mass is given by

$$M_\alpha = m_\alpha - 4G_S\sigma_\alpha + 2K\sigma_\beta\sigma_\gamma, \quad (25)$$

and the effective quark chemical potentials take the form

$$\tilde{\mu}_u = \mu - 4G_V\rho_u - \frac{2}{3}\mu_e, \quad (26)$$

$$\tilde{\mu}_d = \mu - 4G_V\rho_d + \frac{1}{3}\mu_e, \quad (27)$$

$$\tilde{\mu}_s = \mu - 4G_V\rho_s + \frac{1}{3}\mu_e. \quad (28)$$

The quantity  $\tilde{\mu}$  ( $\delta\tilde{\mu}$ ) still has the same form as Eq.(19) [Eq.(20)] with  $g(p) \equiv 1$ . Ignoring the mass difference between the u quark and the d quark (the mass difference is very small [23]), the last term in Eq. (24) has an analytical form which greatly simplifies the numerical calculation. Adopting the variational method, we get the eight nonlinear coupling equations

$$\frac{\partial\Omega}{\partial\sigma_u} = \frac{\partial\Omega}{\partial\sigma_s} = \frac{\partial\Omega}{\partial\Delta} = \frac{\partial\Omega}{\partial\rho_u} = \frac{\partial\Omega}{\partial\rho_d} = \frac{\partial\Omega}{\partial\rho_s} = \frac{\partial\Omega}{\partial\mu_e} = \frac{\partial\Omega}{\partial\mu_8} = 0. \quad (29)$$

Since  $\mu_8$  is near zero around the chiral transition region [23, 24], taking it to zero makes little difference in the calculational result and the nonlinear equations can be reduced to 7.

### C. Numerical calculation and discussion

Similar to the two-flavor case, the vector interaction  $G_V/G_S$  is also taken as a free parameter in the following, and the diquark coupling  $G_D/G_S$  is fixed to the standard value. Because of the contribution from the KMT interaction, the ratio  $G_D/G_S$  from Fierz transformation should be 0.95 rather than 0.75 when only considering the four-quark interaction [6]. Note that in this case the effective four-quark interaction which determines the quark constituent mass in vacuum is  $G_{S'} = G_S - \frac{1}{2}K\sigma_s$ , and the standard value of  $G_D/G_{S'}$  should be 0.75.

The phase diagrams with a multiple critical-point structure for different vector interactions are shown in Fig.7. One can see that these phase diagrams are very similar to Fig.4, the two-flavor case with parameter set 2. This is reasonable since these two models almost reproduce the same constituent quark (u and d) masses and have similar scale parameters. Figure7 indicates that the KMT interaction does not change the possible multiple critical-point structures for the chiral phase transition.

For simplicity, the unstable regions with chromomagnetic instability are not plotted in Fig.7. The calculation of the Meissner mass squared in the 2CSC phase for the two-plus-one-flavor case is straightforward but complicated. Including the s quark should have little effect on the value of the Meissner masses calculated according to the formula for the two-flavor case [22] since the s quark does not take part in Cooper pairing. We can expect that the critical points E, F, and G should still be free from the chromomagnetic instability, as in Figs.2 and 4, since the large strange quark may give a positive contribution rather than a negative one to the Meissner masses squared. As for critical point H, it may be located in the unstable region and could be safe from the instability because the relatively large  $G_V/G_S$  may suppress the unstable region to lower  $T$  and higher  $\mu$ .

Usually, it is argued that the instantons should be screened at large chemical potential and temperature. Therefore, compared to its vacuum value, the coupling constant  $K$  is expected to be reduced around the chiral boundary. For smaller  $K$ , the flavor mixing effect is suppressed and the mass mismatch between the s quark and the u(d) quark becomes larger. Accordingly, the influence of the s quark on the chiral restoration is weakened, and the situation approaches the two-flavor case. On the other hand, with decreasing  $K$ , the u(d) quark mass also decreases since the contribution from the s quark mass is reduced. This means the first-order chiral restoration will be weakened when decreasing  $K$ . Correspondingly, the COE region should be more easily formed with the influence of the vector interaction and the neutral CSC phase, which favors the multiple critical-point structures or crossover for chiral restoration at low temperature.

Of course, the produced u(d) quark vacuum constituent masses with different model parameters of the two-plus-one-flavor NJL model may range from 300-400 MeV, which are all phenomenologically acceptable just as the two-flavor case. Then, one can expect that all the critical-point structures found in Sec. II should also appear in the two-plus-one-flavor case, even considering the axial anomaly interaction term.

## IV. CONCLUSIONS AND OUTLOOK

In this paper, we have explored the effect of the repulsive vector-vector interaction combined with electric-charge neutrality in  $\beta$  equilibrium on the chiral phase and CSC phase transitions within both two-flavor and two-plus-one-flavor NJL models.

For the two-flavor case with the presence of the neutral CSC phase, we demonstrated that, with the help of the repulsive vector interaction, there always exists a parameter window in the NJL models which favors the appearance of a multiple chiral critical-point structure for a wide range of the vacuum quark mass, i.e., from 300 MeV to 400 MeV. Besides the two- and three-critical-points structures found in [9, 21] and [21], respectively, we have shown for the first time that a four-critical-points structure of the QCD phase diagram can be realized; such a multiple critical-point structure is caused by the joint effect of positive  $\mu_e$  and  $G_V$ . Because the dynamical strange quark mass is still relatively large near the boundary of the chiral transition, the multiple critical-point structures present in the two-flavor case also appear in the two-plus-one-flavor case. For the intermediate diquark coupling case, the number of critical points changes as  $1 \rightarrow 2 \rightarrow 4 \rightarrow 2 \rightarrow 0$  with an increasing vector coupling in the two-plus-one-flavor NJL model. In general, one can expect that different model parameters may possibly give other order of the number of the critical points as the vector coupling is increased.

Although our analysis is based on a low-energy effective model which inherently has, more or less, a parameter dependence, we have seen that the physical mechanism to realize the multiple critical-point structure is solely dependent on the basic ingredients of the effective quark dynamics and thermodynamics. Therefore, we believe that the results obtained in the present work should be taken seriously and examined in other effective models of QCD, or hopefully lattice QCD simulations. Our result also has a meaningful implication for the study of phase transitions in condensed matter physics. That means some external constraints enforced on the system can lead to the formation or expansion of the coexisting phase, and the competition between two order parameters can give rise to multiple critical points.

Last but not least, we emphasize that we have shown for the first time that the repulsive vector interaction which should generically exist between the quarks does suppress the chromomagnetic instability related to the asymmetric homogeneous 2CSC phase. With increasing vector interaction, the unstable region associated with chromomagnetic instability shrinks towards lower temperatures and higher chemical potentials. This means that the vector interaction can partially or even totally resolve the chromomagnetic instability problem.

Note that to cure the chromomagnetic instability, inhomogeneous asymmetric color superconductivity phases such as the LOFF phase and the gluonic phase were proposed in the literature. For the inhomogeneous phase, beside the condensate  $\langle \bar{\psi}\gamma_0\psi \rangle$ , there is no reason to rule out the appearance of another new condensate,  $\langle \bar{\psi}\vec{\gamma}\psi \rangle$ , when considering the vector interaction. The effect of both the timelike vector condensate and the spacelike condensate on the asymmetric inhomogeneous CSC phase will be reported in our future work[48].

### Acknowledgments

We acknowledge Kenji Fukushima for useful discussion. One of the authors ( Z. Z. ) is grateful for the support from the Grants-in-Aid provided by Japan Society for the Promotion of Science (JSPS). This work was partially supported by a Grant-in-Aid for Scientific Research by the Ministry of Education, Culture, Sports, Science and Technology (MEXT) of Japan (No. 20540265 and No. 19-07797), by Yukawa International Program for Quark-Hadron Sciences, and by the Grant-in-Aid for the global COE program “ The Next Generation of Physics, Spun from Universality and Emergence ” from MEXT.

- 
- [1] M. Asakawa and K. Yazaki, Nucl. Phys. A **504**, 668 (1989).
  - [2] A. Barducci, R. Casalbuoni, S. De Curtis, R. Gatto and G. Pettini, Phys. Lett. B **231**, 463 (1989); Phys. Rev. D **49**, 426 (1994).
  - [3] As a review, see, M. A. Stephanov, Prog. Theor. Phys. Suppl. **153**, 139 (2004) [Int. J. Mod. Phys. A **20**, 4387 (2005)]; PoS **LAT2006**, 024 (2006) [arXiv:hep-lat/0701002].
  - [4] K. Rajagopal and F. Wilczek, arXiv:hep-ph/0011333.
  - [5] D. H. Rischke, Prog. Part. Nucl. Phys. **52**, 197 (2004) [arXiv:nucl-th/0305030].
  - [6] M. Buballa, Phys. Rept. **407**, 205 (2005) [arXiv:hep-ph/0402234].
  - [7] M. G. Alford, A. Schmitt, K. Rajagopal and T. Schafer, arXiv:0709.4635 [hep-ph].
  - [8] M. G. Alford, K. Rajagopal and F. Wilczek, Nucl. Phys. B **537**, 443 (1999) [arXiv:hep-ph/9804403].
  - [9] M. Kitazawa, T. Koide, T. Kunihiro and Y. Nemoto, Prog. Theor. Phys. **108**, 929 (2002) [arXiv:hep-ph/0207255].
  - [10] S. Klimt, M. Lutz and W. Weise, Phys. Lett. B **249**, 386 (1990).
  - [11] M. Buballa, Nucl. Phys. A **611**, 393 (1996) [arXiv:nucl-th/9609044].
  - [12] N. Evans, S. D. H. Hsu and M. Schwetz, Nucl. Phys. B **551**, 275 (1999).
  - [13] T. Schäfer and F. Wilczek, Phys. Lett. B **450**, 325 (1999).
  - [14] T. Schäfer and E. Shuryak, Rev. Mod. Phys. **70**, 323 (1998).
  - [15] C. D. Roberts and A. G. Williams, Prog. Part. Nucl. Phys. **33** (1994) 477; P. C. Tandy, Prog. Part. Nucl. Phys. **39** (1997) 117.
  - [16] D. Ebert and M. K. Volkov, Z. Phys. C **16**, 205 (1983).
  - [17] D. Ebert and H. Reinhardt, Nucl. Phys. B **271**, 188 (1986).
  - [18] M. Takizawa, K. Tsushima, Y. Kohyama and K. Kubodera, Prog. Theor. Phys. **82**, 481 (1989); S. Klimt, M. Lutz, U. Vogl and W. Weise, Nucl. Phys. A **516**, 429 (1990).
  - [19] T. Hatsuda, M. Tachibana, N. Yamamoto and G. Baym, Phys. Rev. Lett. **97**, 122001 (2006) [arXiv:hep-ph/0605018]; Phys. Rev. D **76**, 074001 (2007) [arXiv:0704.2654 [hep-ph]].
  - [20] T. Schafer and F. Wilczek, Phys. Rev. Lett. **82**, 3956 (1999) [arXiv:hep-ph/9811473]; M. G. Alford, J. Berges and K. Rajagopal, Nucl. Phys. B **558**, 219 (1999) [arXiv:hep-ph/9903502].
  - [21] Z. Zhang, K. Fukushima and T. Kunihiro, Phys. Rev. D **79**, 014004 (2009) [arXiv:0808.3371 [hep-ph]].
  - [22] M. Huang and I. A. Shovkovy, Phys. Rev. D **70**, 051501(R) (2004) [arXiv:hep-ph/0407049]; *ibid.* D **70**, 094030 (2004) [arXiv:hep-ph/0408268].
  - [23] S. B. Ruester, V. Werth, M. Buballa, I. A. Shovkovy and D. H. Rischke, Phys. Rev. D **72**, 034004 (2005) [arXiv:hep-ph/0503184].
  - [24] H. Abuki and T. Kunihiro, Nucl. Phys. A **768**, 118 (2006) [arXiv:hep-ph/0509172].
  - [25] M. Kobayashi and T. Maskawa, Prog. Theor. Phys. **44**, 1422 (1970); M. Kobayashi, H. Kondo and T. Maskawa, Prog. Theor. Phys. **45**, 1955 (1971); G. 't Hooft, Phys. Rev. **D14**, 3432 (1976); Phys. Rept. **142**, 357 (1986).
  - [26] T. Hatsuda and T. Kunihiro, Phys. Rev. Lett. **55**, 158 (1985); Phys. Rept. **247**, 221 (1994) [arXiv:hep-ph/9401310].
  - [27] S. P. Klevansky, Rev. Mod. Phys. **64**, 649 (1992).

- [28] M. G. Alford, K. Rajagopal and F. Wilczek, Phys. Lett. B **422**, 247 (1998) [arXiv:hep-ph/9711395].
- [29] S. M. Schmidt, D. Blaschke and Yu. L. Kalinovsky, Phys. Rev. C **50**, 435 (1994).
- [30] R. D. Bowler and M. C. Birse, Nucl. Phys. A **582**, 655 (1995) [arXiv:hep-ph/9407336].
- [31] D. Blaschke, G. Burau, Yu. L. Kalinovsky, P. Maris and P. C. Tandy, Int. J. Mod. Phys. A **16**, 2267 (2001) [arXiv:nucl-th/0002024].
- [32] D. Gomez Dumm, D. B. Blaschke, A. G. Grunfeld and N. N. Scoccola, Phys. Rev. D **73**, 114019 (2006) [arXiv:hep-ph/0512218].
- [33] D. N. Aguilera, D. Blaschke, H. Grigorian and N. N. Scoccola, Phys. Rev. D **74**, 114005 (2006) [arXiv:hep-ph/0604196].
- [34] H. Grigorian, Phys. Part. Nucl. Lett. **4**, 223 (2007) [arXiv:hep-ph/0602238].
- [35] O. Kiriya, Phys. Rev. D **74**, 114011 (2006) [arXiv:hep-ph/0609185].
- [36] M. Alford and K. Rajagopal, JHEP **0206**, 031 (2002) [arXiv:hep-ph/0204001]; A. W. Steiner, S. Reddy and M. Prakash, Phys. Rev. D **66**, 094007 (2002) [arXiv:hep-ph/0205201].
- [37] I. Giannakis and H. C. Ren, Phys. Lett. B **611**, 137 (2005) [arXiv:hep-ph/0412015].
- [38] E. V. Gorbar, M. Hashimoto and V. A. Miransky, Phys. Lett. B **632**, 305 (2006) [arXiv:hep-ph/0507303]; Phys. Rev. Lett. **96**, 022005 (2006) [arXiv:hep-ph/0509334]; Phys. Rev. D **75**, 085012 (2007) [arXiv:hep-ph/0701211].
- [39] O. Kiriya, D. H. Rischke and I. A. Shovkovy, Phys. Lett. B **643**, 331 (2006) [arXiv:hep-ph/0606030];
- [40] L. He, M. Jin and P. Zhuang, Phys. Rev. D **75**, 036003 (2007) [arXiv:hep-ph/0610121].
- [41] K. Fukushima, Phys. Rev. D **72**, 074002 (2005) [arXiv:hep-ph/0506080].
- [42] M. Kitazawa, D. H. Rischke and I. A. Shovkovy, Phys. Lett. B **637**, 367 (2006) [arXiv:hep-ph/0602065].
- [43] V. Bernard, R. L. Jaffe and U. G. Meissner, Phys. Lett. B **198**, 92 (1987).
- [44] T. Hatsuda and T. Kunihiro, Phys. Lett. B **198**, 126 (1987).
- [45] T. Kunihiro and T. Hatsuda, Phys. Lett. B **206**, 385 (1988); Erratum-ibid. **210**, 278 (1988); T. Kunihiro, Phys. Lett. B **219**, 363 (1989).
- [46] V. Bernard, R. L. Jaffe and U. G. Meissner, Nucl. Phys. B **308**, 753 (1988).
- [47] P. Rehberg, S. P. Klevansky and J. Hufner, Phys. Rev. C **53**, 410 (1996) [arXiv:hep-ph/9506436].
- [48] Z. Zhang and T. Kunihiro( unpublished ).